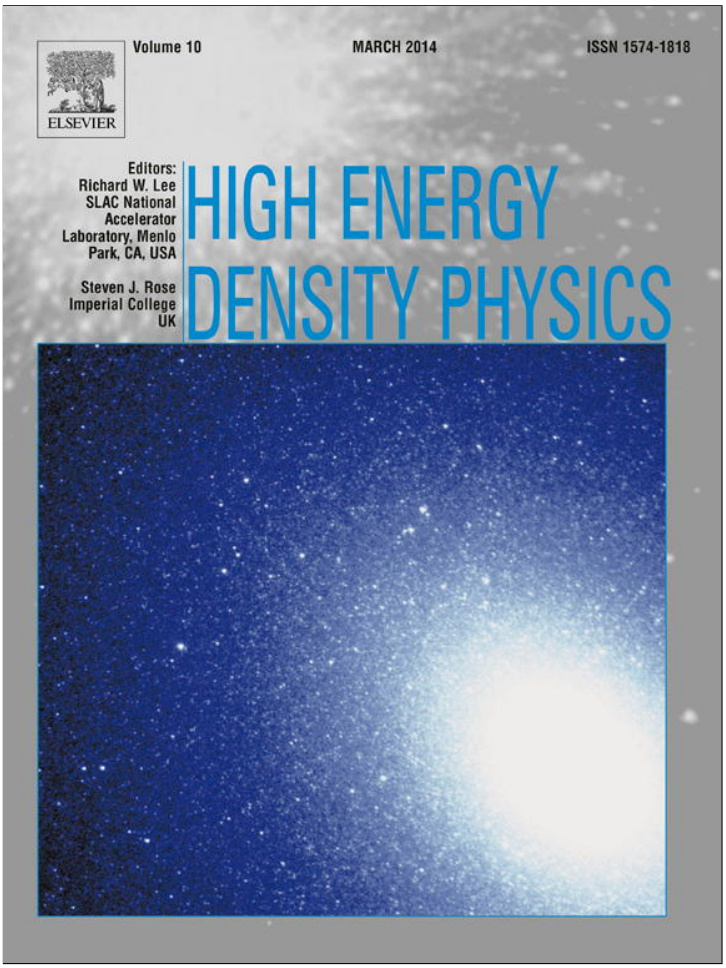

High Energy Density Physics 10 (2014) 56–60

Contents lists available at ScienceDirect

High Energy Density Physics

journal homepage: www.elsevier.com/locate/hedp

Determination of magnetic fields based on the Zeeman effect in regimes inaccessible by Zeeman-splitting spectroscopy

R. Doron [a,*], D. Mikitchuk [a], C. Stollberg [a], G. Rosenzweig [a], E. Stambulchik [a], E. Kroupp [a], Y. Maron [a], D.A. Hammer [b]

[a] Faculty of Physics, Weizmann Institute of Science, Rehovot 76100, Israel
[b] Laboratory of Plasma Studies, Cornell University, Ithaca, NY 14853, USA

ARTICLE INFO

Article history:
Received 7 October 2013
Accepted 7 October 2013
Available online 17 October 2013

Keywords:
Magnetic-field determination
Zeeman spectroscopy
Stark broadening

ABSTRACT

We discuss the limits of applying spectroscopic methods for the determination of magnetic fields that are based on the Zeeman effect and allow for extending the field diagnostics to conditions in which the Zeeman-split pattern is not resolvable. We analyze the diagnostic limits in terms of the minimum magnetic field that can be determined for a given Lorentzian line-width. This form of analysis is useful since the Lorentzian profile corresponds to the Stark broadening of isolated spectral lines that is often the main mechanism of smearing out the Zeeman-split patterns in high-energy-density plasmas. The analysis is performed for the ^2S–^2P atomic system. It is shown that the curves that define the limits of the diagnostic methods in the magnetic-field Lorentzian-width plane, are linear for a wide range of parameters and can be obtained by employing simple expressions that are useful for planning experiments and diagnostic systems.

1. Introduction

Plasma conditions that are typical of high-energy-density (HED) systems often render the common Zeeman-splitting magnetic-field diagnostic impossible. The high densities and high ion velocities result in broad spectral line-shapes that smear out the Zeeman-split patterns, even when polarization techniques are employed to remove the π-Zeeman components from the spectrum. Moreover, when the magnetic-field magnitude and direction vary in time or over spatial scales that are below the diagnostic system resolution (here denoted as "non-directional field"), polarization techniques are either inapplicable or provide ambiguous results. Alternative approaches to Zeeman spectroscopy, mainly employed for the determination of self-generated fields in laser-produced plasmas, are based on polarimetry, e.g., see Refs. [1–4], or proton-beam deflectometry, e.g., see Refs. [5–7]. Yet, expanding the usefulness of spectroscopic tools based on the Zeeman effect to HED conditions is attractive since this technique does not require a probe beam and its reliability is well established.

The only available spectroscopic approach for a reliable determination of non-directional fields is based on the comparison of line shapes of different fine-structure components of the same multiplet [8]. This approach was recently demonstrated [9] for measuring the fields in a laser-produced plasma in an externally applied magnetic field and has also been used in a wire explosion experiment [10]. Different techniques, applicable only when a preferred direction of the magnetic field exists, are based on observing the differences in the spectral-line profiles or spectral positions measured simultaneously in different polarizations. This approach was used to determine magnetic-fields in z-pinch experiments [11,12]. Unlike straightforward diagnostics based on observed Zeeman splitting, applying these techniques, that extend the applicability of Zeeman-based spectroscopy, requires detailed line-shape modeling and/or cumbersome experimental arrangements to enable simultaneous measurements of the emission in different polarizations. It is therefore useful to identify the plasma and magnetic-field regimes in which these techniques can be applied.

In this report, we identify regions in the magnetic-field line-width plane (for Lorentzian line shapes), in which the different spectroscopic techniques are applicable. These regions are obtained by extensive calculations of Zeeman Lorentzian-broadened patterns for selected transitions, and by defining practical criteria that should enable extracting the magnetic field from the line-shape analysis.

2. Brief description of the diagnostic methods

We first discuss the method presented in Ref. [8], henceforth the Fine-Structure-Components method, that utilizes the comparison

* Corresponding author.
E-mail address: ramy.doron@weizmann.ac.il (R. Doron).

1574-1818/$ – see front matter © 2013 Elsevier B.V. All rights reserved.
http://dx.doi.org/10.1016/j.hedp.2013.10.004

of line shapes of two different fine-structure components of the same atomic multiplet. It is based on the fact that these components undergo different Zeeman splittings in a magnetic field, while the other line-broadening mechanisms, namely the Stark and the Doppler effects, and the instrumental broadening, are practically identical for the two components. Therefore, if these two multiplet components can be recorded simultaneously, the difference between the line shapes, that (in the absence of opacity) is only due to the magnetic field, can be used for the field determination. A unique advantage of the method is its applicability to non-directional magnetic fields, since it does not rely on the emission polarization properties. It is noteworthy that the differences in the line-widths are not the same for the two different polarization components (π and σ), which may contribute to the uncertainty in the measurement if no information on the field direction is available [9].

Generally, ^2S–^2P type transitions are favorable candidates for the diagnostics since the relative line-width difference between the doublet components ($^2S_{1/2} - {}^2P_{1/2}$ and $^2S_{1/2} - {}^2P_{3/2}$) is most sensitive to the magnetic field. Ideally, the recorded spectral features of the two fine-structure components are well separated, so they can be normalized and shifted to a common central wavelength, enabling a straightforward line-shape comparison; the line-width difference serves as a clear indication of the magnetic field. However, in practice, large line-broadening may result in partial overlapping of the fine-structure features that prohibits such a straightforward line-shape comparison, as demonstrated in Fig. 1. The figure presents a simulation of the Zeeman pattern of the 3*s*–3*p* doublet in C IV for a magnetic field of 10 T, and the convolution of the pattern with a 5-Å FWHM Lorentzian (corresponding to an electron density, $n_e = 10^{18}$ cm^{-3}, e.g., see Ref. [13]). Comparison of the shapes of the fine-structure components is impossible since the exact line-shape of each component is unknown and thus the two features cannot be deconvolved. In such cases, the magnetic field determination is accomplished by detailed line-shape modeling, which is made possible using the constraints that the contributions of the various line-broadening mechanisms to the multiplet components, except that of the Zeeman effect, are the same. Employing this method also provides information on the plasma density [9].

Two different methods, based on the emission polarization properties, are applicable when a dominant direction of the magnetic field exists. In the first technique, useful for lines of sight that are approximately perpendicular to the magnetic-field direction, henceforth to be called the Polarization-Perpendicular method, the field is determined by detecting the relative contributions of the π and σ Zeeman components to the observed line shape, e.g., see Ref. [11]. In the second technique, useful for lines of sight parallel to the magnetic field, henceforth to be called the Polarization-Parallel method, the left and right circular polarizations of the σ-Zeeman components allow each of these components to be recorded separately, e.g., see Ref. [12]. The wavelength separation is then used for the field determination. Besides their inapplicability for the determination of non-directional fields, these techniques bear another disadvantage arising from the need to record simultaneously the emission in the different polarizations, resulting in lower signal-to-noise ratios. On the other hand, when applicable, the polarization techniques provide a higher sensitivity, as shown in Section 3.

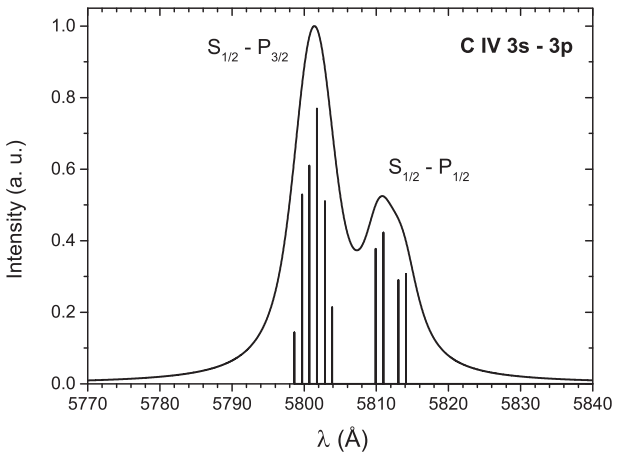

Fig. 1. Zeeman effect of the C IV 3*s*–3*p* doublet, calculated for a magnetic field of 10 T and convolved with a 5-A FWHM Lorentzian. Also shown is the Zeeman pattern with no line broadening.

3. Application regimes

In HED plasmas, often the difficulty in applying traditional Zeeman-splitting spectroscopy arises from the Stark contribution to the line widths of isolated lines. Therefore, we choose to present the application regimes of the diagnostic methods, in the magnetic-field Lorentzian-line-width plane; here the Lorentzian profile corresponding to the Stark broadening. For comparison, we also give the application regime for the Zeeman-splitting diagnostics. Detailed information is given for utilizing the ^2S–^2P doublet for two selected ions, Al III and O VI, but we also give simple expressions that give estimates for the diagnostic limits for this type of transition in other ions.

The applicability limit of the Zeeman-splitting diagnostics is determined by the ability to resolve the Zeeman-split components using the Rayleigh criterion and assuming a line of sight parallel to the magnetic field. For the Fine-Structure-Components method we determine the applicability limit by the condition that the relative line-width difference, $\Delta\tilde{w}$, is larger than 10%, where $\Delta\tilde{w}$ is defined by:

$$\Delta\tilde{w} = \frac{2\left(w_{1/2} - w_{3/2}\right)}{w_{1/2} + w_{3/2}}, \tag{1}$$

and $w_{1/2}$ and $w_{3/2}$ are the line widths of the $^2S_{1/2}$–$^2P_{1/2}$ and $^2S_{1/2}$–$^2P_{3/2}$ components, respectively. The calculations are performed assuming the line of sight is perpendicular to the magnetic field; however assuming a line-of-sight parallel to the field gives very similar results. Similarly, the applicability limit of the Polarization-Perpendicular method is determined by the condition that the line-width difference of the $^2S_{1/2}$–$^2P_{1/2}$ transition, measured in orthogonal polarizations, i.e., when viewed perpendicular to the field, is larger than 10%. This value of 10% width-difference is based on previous successful measurements [9,11]. For the Polarization-Parallel method, with its applicability limit determined by the uncertainty in the spectral position of the peak of each of the components relative to the magnetic-field induced shift, we choose the condition that the induced shift is larger than 10% of the line width. Clearly, higher-quality experimental data may extend the limits of these diagnostics.

Calculation of the Zeeman-split pattern for the ^2S–^2P transitions is performed in the *LS* approximation by diagonalizing a Hamiltonian consisting of the zero-order Hamiltonian, and the *LS* and magnetic-field interaction terms:

$$H = H_0 + \xi\vec{L}\cdot\vec{S} + (L_z + 2S_z)\mu_B B. \tag{2}$$

The coefficient ξ is found using published energy levels [14]. Each of the Zeeman components is then assigned a Lorentzian shape. Relevant matrix elements in the (l, m_l, s, m_s) representation can be found elsewhere, e.g., in Ref. [15].

Figs. 2 and 3 present the application regimes of the diagnostic methods for the Al III $4s\,^2S_{1/2}$–$4p\,^2P_{1/2,3/2}$ (5969 & 5722 Å) and O VI $3s\,^2S_{1/2}$–$3p\,^2P_{1/2,3/2}$ (3811 & 3834 Å) transitions. The curves represent the minimum magnetic field that can be determined by each of the diagnostic methods for a given Lorentzian width. For example, in Al III (see Fig. 2), for a Lorentzian width of 5 Å ($n_e \approx 8 \times 10^{17}$ cm^{-3}), using the Zeeman-splitting, and the methods Fine-Structure-Components, Polarization-Perpendicular, and Polarization-Parallel, one can determine minimum magnetic fields of 13, 8, 4 and 2.5 T, respectively. Thus, it is seen that the alternatives to the commonly used Zeeman-splitting diagnostics, allow for extending the magnetic-field spectroscopic determination to significantly larger regimes of fields and densities. The polarization-based techniques, when applicable, provide the broadest application regimes.

One might be tempted to extrapolate the curves representing the diagnostic limits to higher magnetic fields and line widths. However, beyond certain combinations of magnetic fields and line widths, the widths of each of the fine-structure components becomes comparable to the *LS* splitting, resulting in a significant overlapping between the $S_{1/2}$–$P_{1/2}$ and the $S_{1/2}$–$P_{3/2}$ transitions that prohibit the application of the diagnostic methods except for the Polarization-Perpendicular technique. The latter might still be applicable since it can rely on the differences in the spectral shape of the entire doublet recorded in orthogonal polarizations. Estimates of the diagnostic limits due to this effect are denoted in Figs. 2 and 3 by the dashed lines.

It can be seen further from Figs. 2 and 3 that for a wide range of parameters the limits of the diagnostic-application regimes are nearly linear. This linear behavior is due to the fact that the magnetic-field-induced energy-level splitting is both symmetrical around the unperturbed energy level and increases linearly with

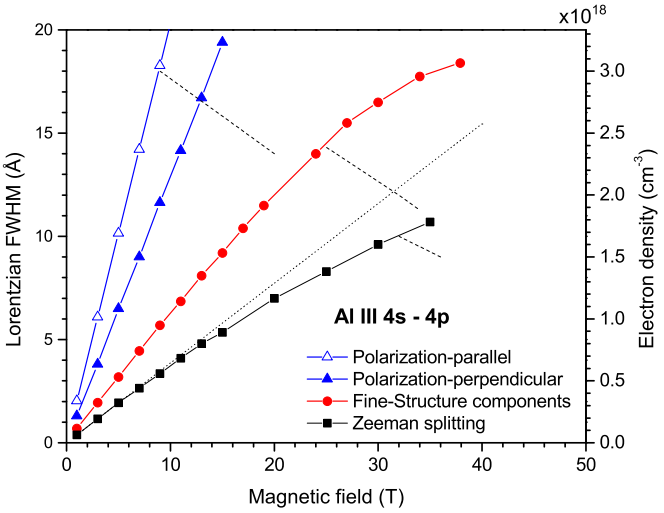

Fig. 2. (Color online) The minimum magnetic field that can be determined for a given Lorentzian line-width (FWHM) by the different diagnostic methods, utilizing the $4s\,^2S$–$4p\,^2P$ doublet in Al III. The limits of the Zeeman-splitting and polarization-based methods refer to $^2S_{1/2}$–$^2P_{1/2}$. The dotted line is a linear extrapolation of the Zeeman-splitting limit, calculated at small line widths and low field magnitudes. The dashed lines represent the approximate limits of each of the diagnostic methods due to significant overlapping between the fine-structure components (except for Polarization-Perpendicular that is not limited – see text). The vertical axis on the right gives the electron density corresponding to the Lorentzian width (calculated using the method in Ref. [16] for an electron temperature at maximum abundance and assuming the entire width is due to the Stark broadening).

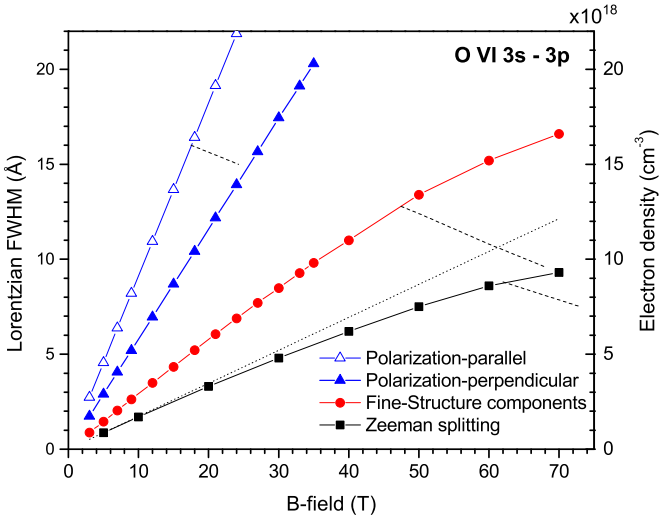

Fig. 3. (Color online) Same as Fig. 2, for the transition $3s\,^2S$–$3p\,^2P$ in O VI.

the magnetic field. While the energy-level splitting is symmetrical, the *intensity* distribution among the Zeeman components becomes increasingly asymmetrical with increasing magnetic field. In addition, overlapping between the fine-structure components, occurring at high densities, tends to increase the asymmetry in the same manner. An asymmetrical spectral feature makes field measurements by the Zeeman-splitting increasingly difficult, as manifested by the deviation from linearity in Figs. 2 and 3. These phenomena are demonstrated in Fig. 4, where the simulated σ component of the Si IV $S_{1/2}$–$P_{1/2}$ transition exhibits an asymmetrical feature, both due to asymmetrical intensity distribution among the Zeeman components and the contribution of the $S_{1/2}$–$P_{3/2}$ red wing. The Rayleigh criterion must then be applied to the intensity at the saddle point at ≈4116.5 Å with respect to the lower-intensity Zeeman component (4120 Å).

As seen in Figs. 2 and 3, the limit of the Fine-Structure-Components method also deviates from linearity, implying lower sensitivity at large line-widths and field amplitudes. However, this occurs due to our choice to determine the application limit by the difference in the FWHM of the fine-structure features, a property that loses its meaning as a test for the actual width when the features become highly asymmetrical at high magnetic fields. The polarization-based methods that depend on detecting robust differences between spectra recorded in different polarizations are less affected by the evolving asymmetries.

The limits of the diagnostic methods in the linear regimes can be obtained analytically and generalized into useful, simple expressions. The calculations are performed in the weak-field approximation, where the magnetic-field perturbation is small compared to the fine-structure separation. The magnetic-field-induced energy-level splitting is then:

$$\Delta E = g_L \mu_B M_J B, \tag{3}$$

where M_J is the projection of the total angular momentum J in the direction of the magnetic field B, μ_B is the Bohr magneton, and g_L the Landé g-factor, given by:

$$g_L = 1 + \frac{J(J+1) + S(S+1) - L(L+1)}{2J(J+1)}, \tag{4}$$

where S and L are, respectively, the total spin and angular momentum of the radiator. According to our assumption of Stark-

dominated line broadening, we describe the spectral intensity of each of the ^2S–^2P doublet components by a sum of its Zeeman components, each represented by a shifted Lorentzian with FWHM of 2γ:

$$f(E) = \sum_i \frac{\alpha_i}{(E-\Delta E_i)^2+\gamma^2}, \tag{5}$$

where ΔE and α are, respectively, the magnetic-field induced energy shift and relative intensity of the different Zeeman components. We note that in principle the energy levels are also Stark-shifted. However, since the Stark shift is the same for all of the doublet Zeeman components, it is unimportant for the present analysis. For $S_{1/2}$–$P_{1/2}$, the calculated energy shifts are $\Delta E = \pm(2/3, 4/3)\mu_B B$ and the corresponding relative intensities are, e.g., see Ref. [17], 1:1 for the perpendicular observation (where both π and σ-components are observed) and 0:1 for the parallel observation (where only the σ-components are observed). For $S_{1/2}$–$P_{3/2}$ $\Delta E = \pm(1/3, 1, 5/3)\mu_B B$ with corresponding relative intensities, for the perpendicular observation 4:3:1, and for parallel observation 0:3:1.

We first consider the limit for the Zeeman splitting. Assuming a symmetrical intensity distribution for the σ components of $S_{1/2}$–$P_{1/2}$ we obtain :

$$f^{\sigma}_{1/2}(E) = \frac{1}{(E+\Delta E)^2+\gamma^2} + \frac{1}{(E-\Delta E)^2+\gamma^2}. \tag{6}$$

To employ the Zeeman-splitting diagnostic we require that the intensity at the saddle point, at $E = 0$, would be lower than 80% of the intensity of one of the peaks at $E = \pm\Delta E$:

$$\frac{2}{\Delta E^2+\gamma^2} < 0.8\left(\frac{1}{\gamma^2+4\Delta E^2}+\frac{1}{\gamma^2}\right). \tag{7}$$

Solving Eq. (7) for $\Delta E = 4/3\ \mu_B B$, we obtain the relation between the line width and the magnetic field for the application limit of the Zeeman splitting:

$$2\gamma < 2.5\mu_B B. \tag{8}$$

To obtain the application limit of the Fine-Structure-Components method (assuming line-of-sight is perpendicular to the magnetic-field direction), we use Eq. (5) to describe the spectral intensity of the $S_{1/2}$–$P_{1/2}$ (the sum of four shifted Lorentzians) and $S_{1/2}$–$P_{3/2}$ (the sum of six shifted Lorentzians) transitions. In the limit where the Zeeman patterns within each of the fine-structure components are unresolved, the peak of each of the fine-structure components is obtained at $E = 0$, the position of the unperturbed doublet component. Using the appropriate energy shifts and the corresponding relative intensities, we obtain for the maxima:

$$f^{\max}_{1/2-1/2}(E) = \frac{2}{4/9(\mu_B B)^2+\gamma^2} + \frac{2}{16/9(\mu_B B)^2+\gamma^2}, \tag{9a}$$

$$f^{\max}_{1/2-3/2}(E) = \frac{8}{1/9(\mu_B B)^2+\gamma^2} + \frac{6}{(\mu_B B)^2+\gamma^2} + \frac{2}{25/9(\mu_B B)^2+\gamma^2}. \tag{9b}$$

These maxima are used to find the widths $w_{1/2}$ and $w_{3/2}$ and to obtain the relation that satisfies the condition $\Delta\tilde{w} > 0.1$ (see Eq. (1)):

$$2\gamma < 4\mu_B B. \tag{10}$$

To obtain the limit for the Polarization-Perpendicular method we begin with a function composed of two unresolved Lorentzians, corresponding to either the two π or the two σ polarizations the $S_{1/2}$–$P_{1/2}$ transition. For $\gamma > \Delta E$, the FWHM of this function can be approximated by:

$$w \approx 2\gamma\left(1+\frac{3}{2}\frac{\Delta E^2}{\gamma^2}\right). \tag{11}$$

To apply the diagnostic that is based on each polarization having a different shift, ΔE_π and ΔE_σ, we require the relative width-difference to be larger than 10%:

$$\frac{2|w_\sigma - w_\pi|}{(w_\sigma + w_\pi)} \approx \frac{3}{2}\frac{\left|\Delta E_\sigma^2 - \Delta E_\pi^2\right|}{\gamma^2} > 0.1. \tag{12}$$

For the $S_{1/2}$–$P_{1/2}$ transition the shifts are: $\Delta E_\pi = 2/3\ \mu_B B$, $\Delta E_\sigma = 4/3\ \mu_B B$, leading to the relation that defines the diagnostic limit:

$$2\gamma < 9\mu_B B. \tag{13}$$

The limit of the Polarization-Parallel method is directly obtained from our choice of the criterion $0.1 \times 2\gamma < \Delta E$. Taking the energy shift of the σ components of $S_{1/2}$–$P_{1/2}$, $\Delta E_\sigma = 4/3\ \mu_B B$ gives the following relation:

$$2\gamma < 13.5\mu_B B. \tag{14}$$

Finally, it is useful to convert these diagnostic limits given through the relation between the line width and the magnetic field in terms of energy units, into practical wavelength units. For the Zeeman-splitting we obtain:

$$2\gamma_\lambda < 1.2 \times 10^{-8}\lambda^2 B, \tag{15a}$$

for the Fine-Structure-Components method we obtain:

$$2\gamma_\lambda < 1.8 \times 10^{-8}\lambda^2 B, \tag{15b}$$

for the Polarization-Perpendicular method we obtain:

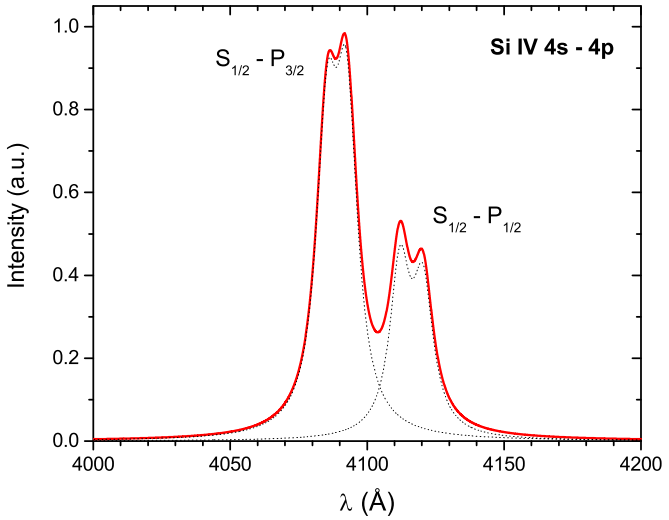

Fig. 4. (Color online) The Zeeman effect for the Si IV 4*s*–4*p*, calculated for a magnetic field of 40 T and convolved with a 9-Å Lorentzian (corresponding to $n_e \approx 2.7 \times 10^{18}$ cm^{-3}). The dotted curves show the line shapes of the fine-structure components separately, demonstrating that the $S_{1/2}$–$P_{3/2}$ "red" wing contributes to the asymmetry of $S_{1/2}$–$P_{1/2}$. (For interpretation of the references to color in this figure legend, the reader is referred to the web version of this article.)

$$2\gamma_\lambda < 4.2 \times 10^{-8}\lambda^2 B, \tag{15c}$$

and for the Polarization-Parallel method, we obtain:

$$2\gamma_\lambda < 6.2 \times 10^{-8}\lambda^2 B. \tag{15d}$$

where the Lorentzian-line width $2\gamma_\lambda$, and the transition wavelength λ, are given in Å, and the magnetic field B is in T. In considering the application limit of the Fine-Structure-Components it should be emphasized that the Stark broadening (in energy units) is the same for all components. Therefore, when the spectrum is presented in wavelength units, the longer wavelength component, $S_{1/2}$–$P_{1/2}$, is wider than the shorter wavelength component, $S_{1/2}$–$P_{3/2}$, also in the absence of the magnetic field. Evidently, this wavelength-width difference is very small in the visible region, but becomes significant in the UV. Eq. (15b) gives the diagnostic limit according to the condition that the Zeeman effect causes the 10% relative-width-difference; whereas the measured relative width difference given in wavelength would be somewhat larger, depending on the transition wavelength.

4. Summary

We discuss the limits of the applications of spectroscopic methods that extend the ability to determine magnetic-field magnitudes to ranges of plasma conditions and magnetic-field properties that are beyond those accessible by the traditional Zeeman-split spectroscopy. The discussion is focused on the limits that arise from the Stark contribution to the spectral line shapes, which is usually the primary mechanism that causes the smearing out of the Zeeman-split pattern in HED plasmas. The diagnostic limits, given in terms of the minimum magnetic field that can be determined for a given Lorentzian-line width, are given for the case of ^2S–^2P doublets that provide high sensitivity to the Zeeman effect. Detailed calculations of the Lorentzian-convolved Zeeman patterns show nearly a linear relation between the Lorentzian width and the minimum measurable field. Deviations from the linear behavior occur at large magnetic fields due to increased asymmetries in the intensity distribution of the Zeeman components, which lead to a lower sensitivity of the diagnostic methods. The diagnostic limits in the linear regime are obtained analytically, yielding simple expressions that are useful for exploring the feasibility of magnetic field measurements and for planning experiments and diagnostic systems.

It is noteworthy that in planning experiments, two additional relevant limitations not discussed here must be considered. The first is the obvious condition that the spectral lines used for the diagnostics should be clearly observed above the continuum. For example, utilizing transitions in the visible-UV region, depending on the line and continuum relative and absolute intensities, such measurements for laboratory plasmas are practically limited to electron densities below $\sim \times 10^{20}$ cm^{-3}. The second important factor is opacity that causes an additional line-broadening. Although the ground level is not involved in the transitions under consideration, opacity effects may be non-negligible in HED plasmas. Using the Fine-Structure-Components and Polarization-Perpendicular methods, opacity effects must be considered for achieving a higher accuracy in the determination of the magnetic field. Moreover, in the case of the Fine-Structure-Components method, opacity effects may cause difficulty in inferring the presence of the magnetic field, since they cause a larger broadening of the $S_{1/2}$–$P_{3/2}$ component than of the $S_{1/2}$–$P_{1/2}$ component. However, detecting the presence of opacity is straightforward, since in the absence of opacity the line intensity ratio between the doublet components $I_{1/2-1/2}$:$I_{1/2-3/2}$ must be 1:2. The Polarization-Parallel technique that provides the highest sensitivity to the magnetic field, is nearly unaffected by opacity since it relies on the line positions rather than on their shapes.

Acknowledgments

This work was supported in part by the Minerva Foundation (Federal German Ministry for Education and Research), by the DOE-Cornell University Excellence Center (U.S.), and by the U.S.–Israel Bi-national Science Foundation (BSF).

References

[1] J.A. Stamper, B.H. Ripin, Faraday-rotation measurements of megagauss magnetic fields in laser-produced plasmas, Phys. Rev. Lett. 34 (1975) 138–141.
[2] M. Borghesi, A.J. MacKinnon, A.R. Bell, R. Gaillard, O. Willi, Megagauss magnetic field generation and plasma jet formation on solid targets irradiated by an ultraintense picosecond laser pulse, Phys. Rev. Lett. 81 (1998) 112–115.
[3] M. Tatarakis, I. Watts, F.N. Beg, E.L. Clark, A.E. DaDangor, A. Gopal, M.G. Haines, P.A. Norreys, U. Wagner, M.-S. Wei, et al., Laser technology: measuring huge magnetic fields, Nature 415 (2002), 280.
[4] S.N. Bland, D.J. Ampleford, S.C. Bott, A. Guite, G.N. Hall, S.M. Hardy, S.V. Lebedev, P. Shardlow, A. Harvey-Thompson, F. Suzuki, K.H. Kwek, Use of faraday probing to estimate current distribution in wire array z pinches, Rev. Sci. Instrum. 77 (2006) 10E315.
[5] C.K. Li, F.H. Séguin, J.A. Frenje, J.R. Rygg, R.D. Petrasso, R.P.J. Town, P.A. Amendt, S.P. Hatchett, O.L. Landen, A.J. Mackinnon, P.K. Patel, V.A. Smalyuk, T.C. Sangster, J.P. Knauer, Measuring e and b fields in laser-produced plasmas with monoenergetic proton radiography, Phys. Rev. Lett. 97 (2006) 135003.
[6] P.M. Nilson, L. Willingale, M.C. Kaluza, C. Kamperidis, S. Minardi, M.S. Wei, P. Fernandes, M. Notley, S. Bandyopadhyay, M. Sherlock, R.J. Kingham, M. Tatarakis, Z. Najmudin, W. Rozmus, R.G. Evans, M.G. Haines, A.E. Dangor, K. Krushelnick, Magnetic reconnection and plasma dynamics in two-beam laser-solid interactions, Phys. Rev. Lett. 97 (2006) 255001.
[7] N.L. Kugland, D.D. Ryutov, C. Plechaty, J.S. Ross, H.-S. Park, Invited article: relation between electric and magnetic field structures and their proton-beam images, Rev. Sci. Instrum. 83 (2012) 101301.
[8] E. Stambulchik, K. Tsigutkin, Y. Maron, Spectroscopic method for measuring plasma magnetic fields having arbitrary distributions of direction and amplitude, Phys. Rev. Lett. 98 (2007) 225001.
[9] S. Tessarin, D. Mikitchuk, R. Doron, E. Stambulchik, E. Kroupp, Y. Maron, D. Hammer, V. Jacobs, J. Seely, B. Oliver, A. Fisher, Beyond Zeeman spectroscopy: magnetic-field diagnostics with Stark-dominated line shapes, Phys. Plasmas 18 (2011) 093301.
[10] K.S. Blesener, S.A. Pikuz, T.A. Shelkovenko, I.C. Blesener, D.A. Hammer, Y. Maron, V. Bernshtam, R. Doron, L. Weingarten, Y. Zarnitsky, Measuring magnetic fields in single aluminum wire plasmas with time-resolved optical spectroscopy, High Energy Density Phys. 8 (2012) 224–226.
[11] G. Davara, L. Gregorian, E. Kroupp, Y. Maron, Spectroscopic determination of the magnetic-field distribution in an imploding plasma, Phys. Plasmas 5 (1998) 1068–1075.
[12] R.P. Golingo, U. Shumlak, D.J.D. Hartog, Note: Zeeman splitting measurements in a high-temperature plasma, Rev. Sci. Instrum. 81 (2010) 126104.
[13] S. Sahal-Bréchot, M. Dimitrijevic, N. Moreau, Stark-b Database, Observatory of Paris, Lerma and Astronomical Observatory of Belgrade, 2012. http://stark-b.obspm. fr.
[14] A. Kramida, Y. Ralchenko, J. Reader, N.A. Team, Nist atomic spectra database (ver. 5.0), National Institute of Standards and Technology, Gaithersburg, MD, 2012 (online), Available: http://physics.nist.gov/asd (11.08.13).
[15] E. Stambulchik, Y. Maron, Effect of high-n and continuum eigenstates on the stark effect of resonance lines of atoms and ions, Phys. Rev. A 56 (1997) 2713–2719.
[16] E. Stambulchik, Y. Maron, Plasma formulary interactive, J. Instrum. 6 (2011) P10009.
[17] R.D. Cowan, The Theory of Atomic Structure and Spectra, University of California Press, 1981.